Title

Chemical upgrade of carbon monoxide to acetate on an atomically dispersed copper catalyst via CO-insertion

Authors

Fu, X
Wang, Y
Shen, H
et al.

Publication Date

2021-07-01

DOI

10.1016/j.mtphys.2021.100418

Peer reviewed

Chemical Upgrade of Carbon Monoxide to Acetate on an Atomically Dispersed Copper Catalyst via CO-insertion

Xianbiao Fu,[†,‡,‖] Yuxuan Wang,[‡,‖] Hao Shen,[‡] Yanan Yu,[†] Fei Xu,[‡] Guangye Zhou,[‡] Wenjun Xie,[‡,§] Ruixuan Qin,[‖] Chaochao Dun,[⊥] Yisheng Liu,[#] Jinghua Guo,[#] Qin Yue,[†] Jeffrey J. Urban,[⊥] Chao Wang,[*,‡] Yijin Kang[*,†]

[†] Institute of Fundamental and Frontier Sciences, University of Electronic Science and Technology of China, Chengdu, Sichuan 610054, China

[‡] Department of Chemical and Biomolecular Engineering, Johns Hopkins University, Baltimore, Maryland 21218, United States

[§] Department of Chemistry, Nankai University, Tianjin 300071, P.R. China

[‖] College of Chemistry and Chemical Engineering, Xiamen University, Xiamen 361005, P.R. China

[⊥] The Molecular Foundry, Lawrence Berkeley National Laboratory, Berkeley, CA, 94720, US

[#] Advanced Light Source, Lawrence Berkeley National Laboratory, Berkeley, California 94720, United States

[‖] These authors contributed equally.

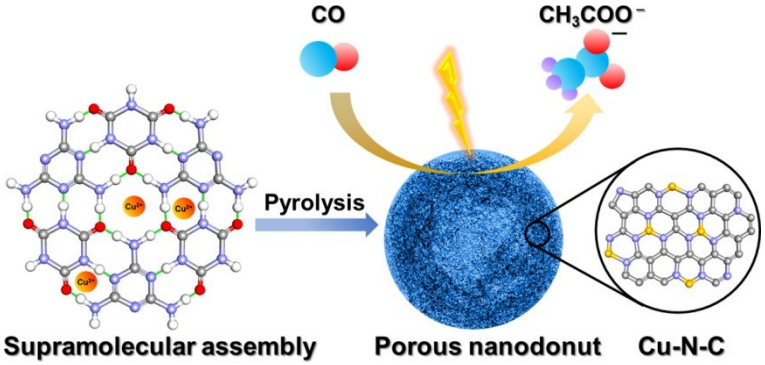

Abstract

Electrochemical conversion of small molecules such as carbon dioxide (CO_2) and carbon monoxide (CO) to high-value multi-carbon products (C_{2+}) offers a chemical upgrade approach for fuels and chemical feedstocks production using renewable energy, in the possible absence of petrochemical industry under the new energy system such as hydrogen economy. Identifying robust and efficient electrocatalysts to selectively produce the C_{2+} products

remains a challenge. Herein, we report a synthetic strategy of atomically dispersing copper atoms on nitrogen-rich porous carbon (Cu-N-C) through pyrolysis of a supramolecular assembly. Benefitting from the unsaturated coordination structure, in KOH electrolyte, the Cu-N-C with a Cu content of 6.9 wt% exhibits a maximum acetate Faradaic efficiency (FE) of 30% with an acetate partial current density as high as 48 mA cm^{-2} in electrochemical CO reduction. Different from the C-C coupling mechanism on metallic copper, we propose a CO insertion mechanism for the acetate production on the single site copper catalyst.

Introduction

The chemical upgrade based on the renewable-energy-driven carbon dioxide reduction reaction (CO_2RR) is a key component to supply necessary chemicals for the new energy system such as hydrogen economy, where the petrochemical industry may no longer exist.[1-8] Copper (Cu) is the only single metal catalyst that is capable of electrocatalytic converting CO_2 or CO into multi-carbon products (C_{2+}) with a considerable selectivity and activity due to its unique d-band center and intermediate strength of CO adsorption.[9-11] It has been proven that CO is a key reaction intermediate for C-C coupling and suppression of the competing hydrogen evolution reaction during the CO_2RR, hence, compared to the direct CO_2RR route, a two-step electrochemical process where CO_2 is first reduced to CO (CO_2-derived CO) and then sequentially reduced to C_{2+}, can effectively improve the current efficiency and the selectivity towards C_{2+} upgrade.[12-16] Many efforts have been devoted towards optimizing the Cu-based electrocatalysts by engineering its composition, dimension, structure, and morphology to lower the energetic barriers for CO_2/CO electroreduction via stabilizing reaction intermediates and transition states.[8, 15, 17-25] Although some progress has been made in the development of more active and selective electrocatalysts, understanding of the structure-activity correlation still faces many challenges. When the Cu nanoparticles size is below 5 nm, the activity and selectivity for H_2 and CO is dramatically increased, which was attributed to the high ratio of low-coordinated surface Cu atoms.[21] The catalytic performance of single-site catalysts (SSCs) is also greatly affected by the surrounding coordination environment.[26-27] Whether Cu-based SSCs can selectively produce C_{2+} products by modulating the coordination environment of Cu sites is still an open challenge. Recently, SSCs have attracted great attention in electrochemical energy conversion,[6, 17, 26, 28-32] yet Cu-based SSCs are rarely explored in the CO_2/CO electroreduction. Cu-based SSCs were reported to usually produce single-carbon compounds such as CO, methane, or methanol in CO_2 electrolysis,[33-37] and Cu-based SSCs for the highly selective production of acetate from CO_2/CO electrolysis has not yet been reported.

Herein, we report a synthetic strategy of atomically dispersing Cu atoms on nitrogen-rich porous carbon (Cu-N-C) via pyrolysis of a supramolecular complex composed of Cu-melamine and cyanuric acid. Aberration corrected high-angle annular dark-field scanning transmission

electron microscopy (HAADF-STEM) and X-ray absorption spectroscopy (XAS) demonstrated that the isolated Cu single atoms were homogenously anchored on the surface of nitrogen-doped porous carbon. Remarkably, in 1 M KOH electrolyte, the Cu-N-C with a Cu content of 6.9 wt% exhibited an acetate Faradaic efficiency (FE) of 30% with an acetate partial current density up to 48 mA cm^{-2} in electrochemical CO reduction. Unlike the C-C coupling mechanism on metallic copper, we believe that the acetate forms via a CO insertion mechanism.

Results and discussion

Synthesis and characterization of Cu-N-C single-site electrocatalysts.

Coordinative pyrolysis strategy has been identified as an effective route to anchor single metal atoms on the nitrogen-doped carbon.[26, 29, 32, 38-41] As shown in Figure 1, the Cu-N-C single-site electrocatalysts were synthesized via pyrolysis of the supramolecular complex composed of Cu-melamine and cyanuric acid under the Ar atmosphere at 550 ℃. The actual Cu contents in the final product of catalysts were determined by the inductively coupled plasma-optical emission spectroscopy (ICP-OES). ICP confirmed the Cu contents of 6.9 wt% and 2.3 wt% in two Cu-N-C catalysts which were prepared by controlling the dose of Cu precursor (Table S1). For control purpose, a blank sample was synthesized without copper precursor and denoted as N-C. X-ray diffraction (XRD) patterns of 6.9 wt% Cu-N-C, 2.3 wt% Cu-N-C, and blank N-C showed that no peaks of metallic Cu can be observed (Figure S1). The peak located at 26° is corresponding to the (002) plane of graphitic carbon.

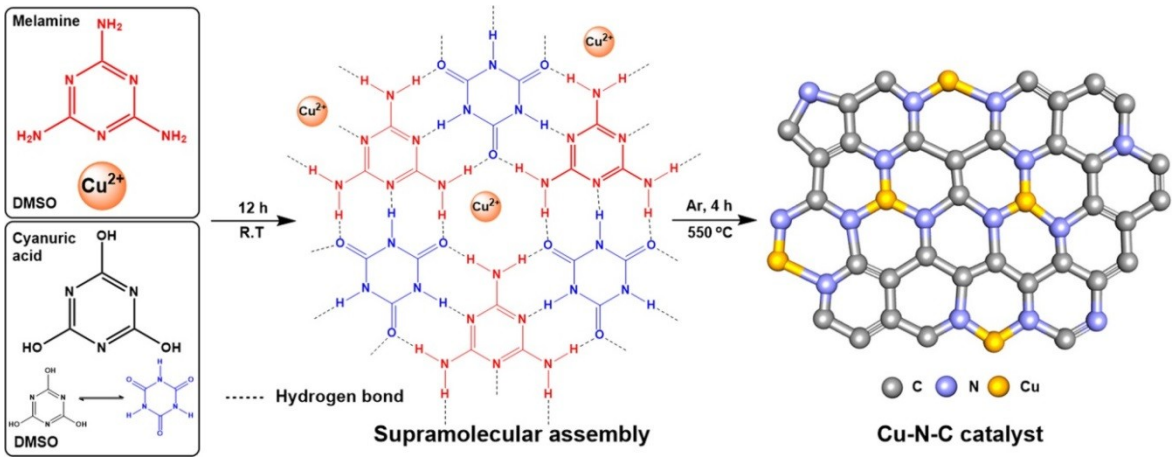

Figure 1. Schematic illustration of the synthesis of Cu-N-C. Cu-melamine and cyanuric acid are assembled into a supramolecular complex through a facile process. The Cu-N-C electrocatalysts are obtained by the pyrolysis of the supramolecular complex under Ar atmosphere.

Transmission electron microscopy (TEM) (Figure 2a, b, and Figure S2) and scanning electron microscopy (SEM) (Figures 2c) images reveal that the Cu-N-C catalyst features a porous nanodonut structure with 1.6 ± 0.2 μm particle size (Figures S3). High-magnification TEM

image (Figure 2b) confirms the absence of any Cu nanoparticles or clusters and the nanoporous structure of Cu-N-C. The HAADF-STEM image of 6.9 wt% Cu-N-C (Figure 2d) shows the homogeneous distribution of high-density Cu single atoms which is enabled by the Z-contrast. The electron energy loss spectra (EELS) clearly exhibit the presence of both N K-edge (Figure S4) and Cu L-edge (Figure 2e), which confirm that Cu atoms are anchored on the porous N-doped carbon. The large-area HAADF-STEM image and corresponding energy dispersive X-ray spectroscopy (EDS) elemental mapping reveal the homogeneous distribution of Cu, N, and C throughout the whole hollow nanodonut (Figure 2f). The electron microscopy techniques were also used to characterize 2.3 wt% Cu-N-C (Figures S5) and showed similar structure and morphology to the 6.9 wt% Cu-N-C. All the above results together evince that the Cu species in N-doped carbon are atomically dispersed.

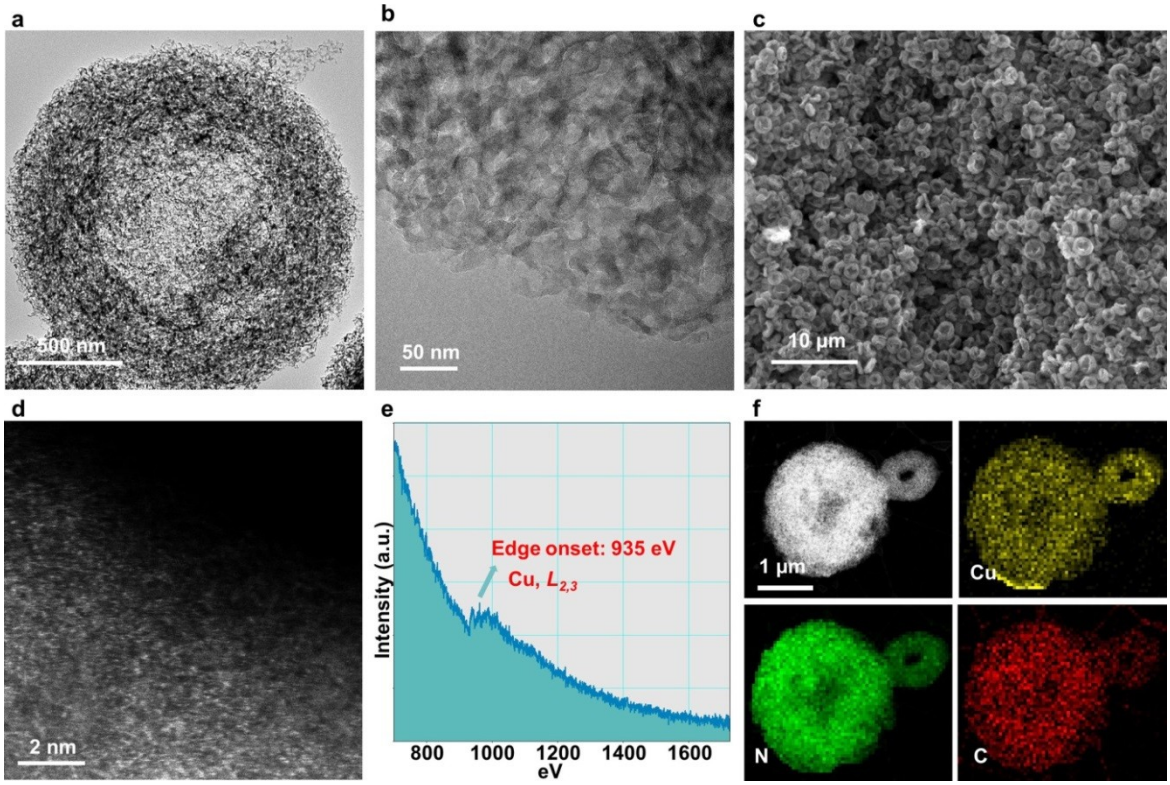

Figure 2. Electron microscopic characterization of the 6.9 wt% Cu-N-C. (a) Low-magnification, and (b) high-magnification TEM images of the 6.9 wt% Cu-N-C. (c) SEM image of 6.9 wt% Cu-N-C. (d) Aberration-corrected HAADF-STEM image, and (e) EELS spectra. (f) HAADF-STEM image and corresponding EDS elemental maps of Cu (yellow), N (green), and C (red). Scale bars: (a) 500 nm, (b) 50 nm, (c) 10μm, (d) 2 nm, and (f) 1 μm.

To explore the structure and coordination environment of Cu species in Cu-N-C at the atomic level, X-ray absorption near edge structure (XANES) and extended X-ray absorption fine structure (EXAFS) measurements were carried out (Figure S6-9 and Table S2). In the Cu L-edge X-ray XANES spectra (Figure 3a), shifts in the energy of the L_3-edge peaks from 930.2 to 930.4 and 930.8 eV for CuO, 2.3 and 6.9 wt% Cu-N-C, respectively, are attributed to the difference

of coordination geometries in the ligand fields, indicating the appearance of Cu^{2+} and Cu^{+} in Cu-N-C.[39] Figure 3b shows the Cu K-edge XANES spectra of Cu-N-C, Cu foil, Cu_2O, and CuO. The absorption edges of Cu-N-C are located between the Cu foil and CuO, which indicate that the oxidized state of Cu atom (i.e. carrying positive charges) in the Cu-N-C is between 0 to 2. The Fourier transformed EXAFS spectra (Figure 3c) of Cu-N-C in which the Cu-Cu bonds at ~ 2.2 Å are absent, confirm that the Cu species anchored in Cu-N-C are atomically dispersed single Cu atoms instead of the Cu clusters or nanoparticles, consistent with the HAADF-STEM observation. The main peaks of Cu-N-C at ~ 1.6 Å are attributed to Cu-N coordination.[34, 38] As illustrated in Figure 3d, the wavelet transforms EXAFS patterns show that the maximum of the wavelet transform of the 6.9 wt% Cu-N-C and Cu foil at around 3.5 and 7.0 $Å^{-1}$ can be assigned to Cu-N and Cu-Cu contribution, respectively. The wavelet transforms EXAFS patterns of the 2.3 wt% Cu-N-C, Cu_2O, and CuO are presented in Figure S6. To confirm the geometric structure of Cu in Cu-N-C, EXAFS fitting was conducted. The fitting parameters are given in Table S2. As shown in Figure 3e, the Fourier transformed EXAFS curve of Cu-N-C can be well fitted with the proposed Cu-N_2 and Cu-N_3 mixed structure shown in Figure 3f.

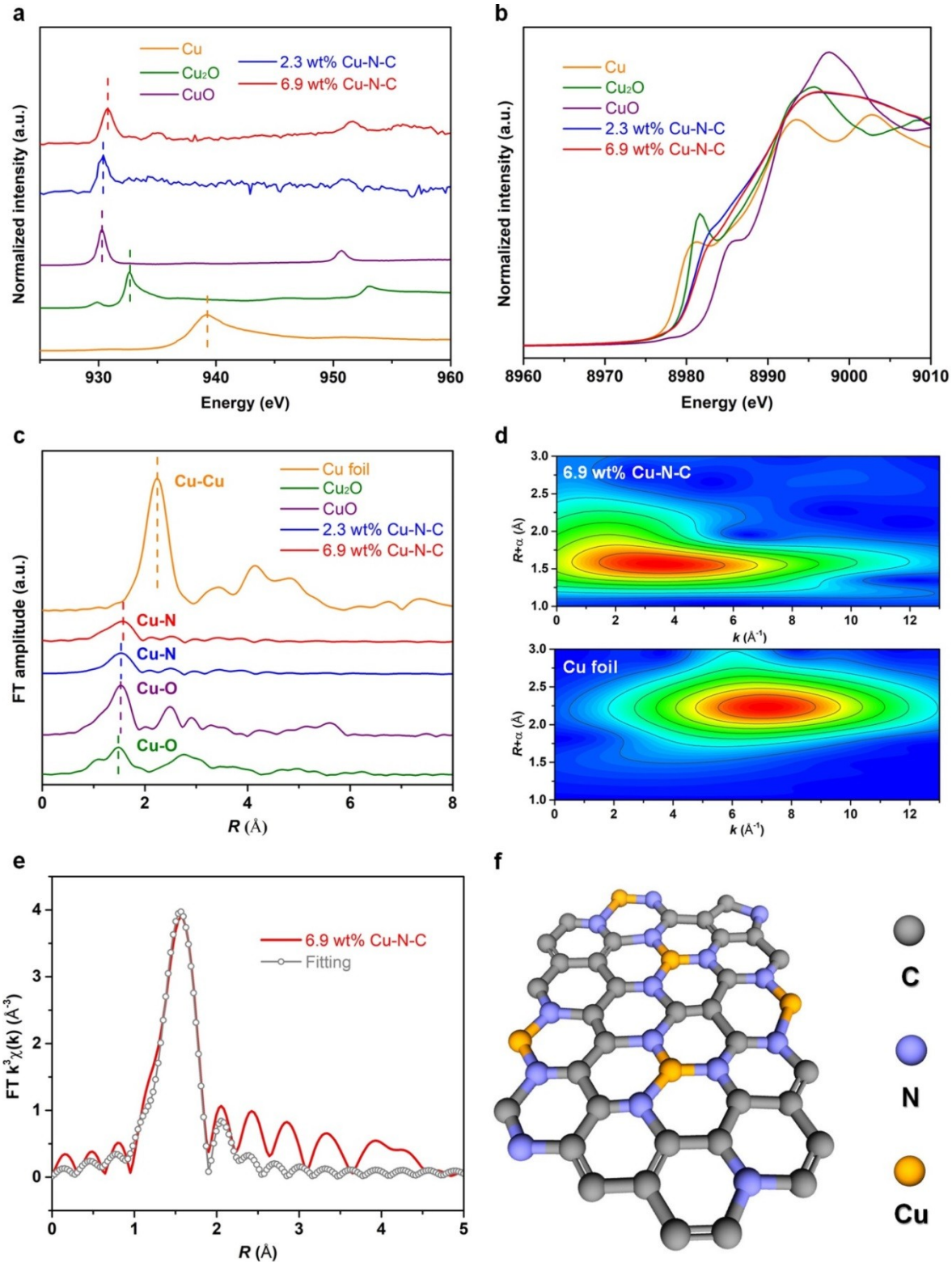

Figure 3. Spectroscopic characterization of Cu-N-C. (a) Normalized Cu L-edge and K-edge (b) XANES spectra of Cu foil, Cu_2O, CuO, 2.3 wt%, and 6.9 wt% Cu-N-C. (c) Fourier transformed EXAFS spectra of Cu K-edge. (d) Wavelet transform plots of 6.9 wt% Cu-N-C (top) and Cu foil (bottom). (e) The corresponding EXAFS fitting curve of 6.9 wt% Cu-N-C. (f) The schematic model of Cu-N-C ($Cu-N_2$ and $Cu-N_3$), Cu (yellow), C (gray), and N (purple).

Electrocatalytic performance

To evaluate the performance of Cu-N-C electrocatalyst in CO electroreduction, a flow-cell electrolyzer was employed (Figure. S10). As described in previous reports,[12, 15] the flow-cell electrolyzer enables a high rate of CO reduction by constructing the tri-phasic interface to overcome inherent mass transport limitations of CO in aqueous electrolyte. The current densities and Faradaic efficiencies (FE) of the CO reduction products are summarized to demonstrate the electrocatalytic performance (Figure. 4). In 1 M KOH, the major C_{2+} products on the 6.9 wt% Cu-N-C were ethylene and acetate with almost no CH_4 produced (i.e. C_{2+} selectivity is ~ 100%), while maximum CH_4 FE of 27% was observed on the 2.3 wt% Cu-N-C (Figure. 4c). To exclude the activity contribution from the support materials, the N-C catalyst was tested as the blank and hydrogen was found as the only product (Figure. S11). Remarkably, a maximum acetate FE of 30% (Figure. 4a) and acetate partial current density up to 48 $mA\,cm^{-2}$ (Figure. 4b) were achieved on the 6.9 wt% Cu-N-C in 1 M KOH, which is the highest selectivity of acetate formation on Cu-based SSCs. The 2.3 wt% Cu-N-C catalyst prefers CH_4 production and suppresses the acetate formation (Figure. 4c), which indicates that the key intermediates *CHO and *COH formation are a pair of competing parallel pathways. In other words, the catalyst with a relatively low density of Cu sites prefers to produce *CHO intermediate for CH_4 formation, while catalyst with a high density of Cu sites tends to generate *COH for acetate production. Comparing the Figure. 4a and c, the 6.9 wt% Cu-N-C catalyst can suppress the competing hydrogen evolution reaction more than 2.3 wt% Cu-N-C, suggesting that more active sites in 6.9 wt% Cu-N-C catalyst are used for CO reduction. To characterize whether the morphology and structure of the Cu-N-C catalyst changed after the electrolysis, electron microscopy and XRD were employed. Post-reaction XRD pattern of the 6.9 wt% Cu-N-C catalyst supported on gas diffusion electrode (GDE) shows no metallic copper diffraction peak (Figure S12), while EELS of Cu L-edge (Figure S13) confirms the presence of Cu element. After electrocatalysis, the HAADF-STEM image of the 6.9 wt% Cu-N-C catalyst (Figure S14) also shows an atomically homogeneous distribution of high-density Cu single sites anchored on nitrogen-doped carbon materials. The presented results confirm the structural stability of the Cu-N-C catalyst for CO electroreduction.

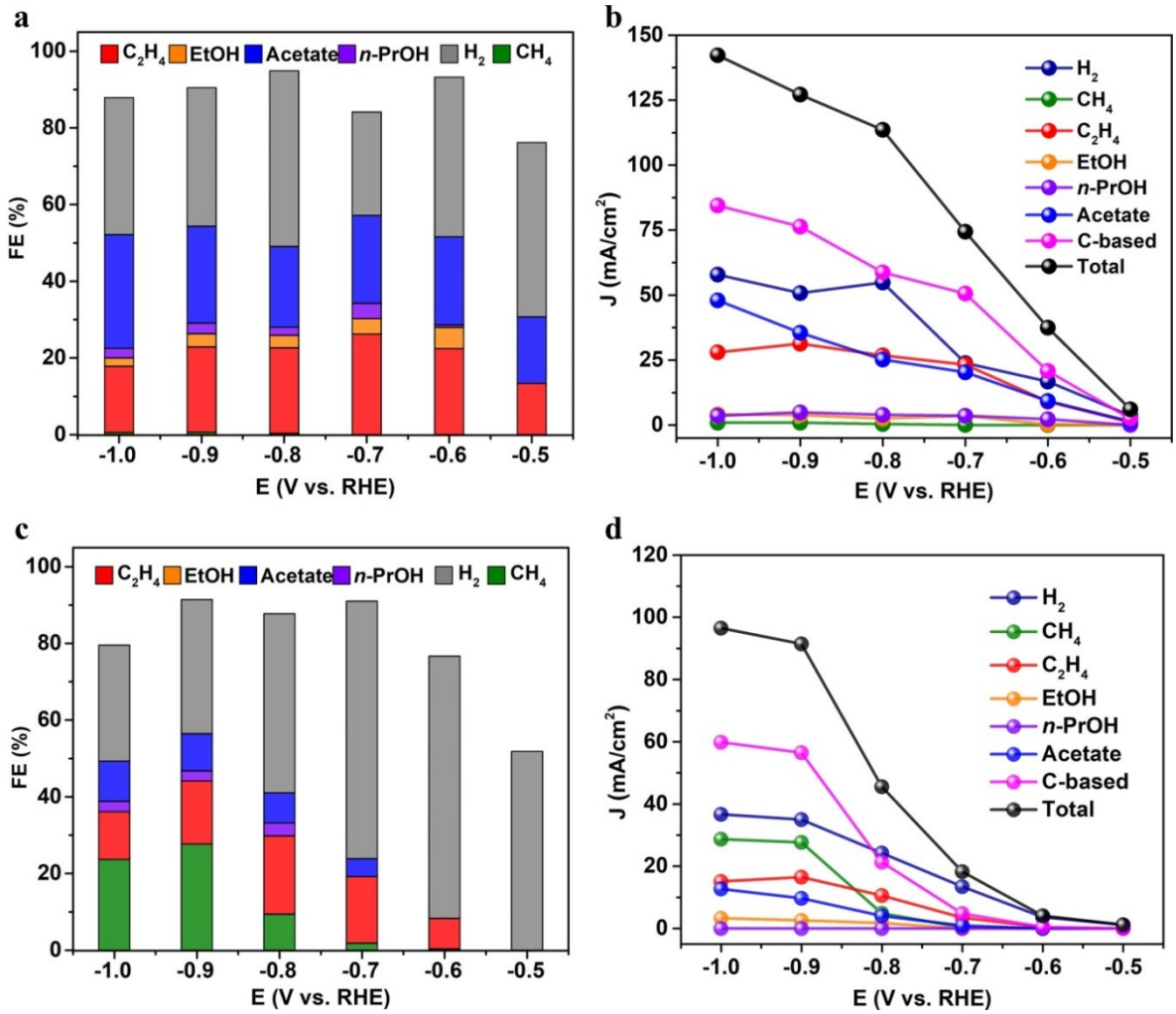

Figure 4. CO electroreduction performance of Cu-N-C. (a) Faradaic efficiency (FE) and total current densities (geometric area) (b) for electroreduction of CO on 6.9 wt% Cu-N-C in 1 M KOH. (c) Faradaic efficiency (FE) and total current densities (d) for CO electroreduction on 2.3 wt% Cu-N-C in 1 M KOH.

Based on the high selectivity of acetate formation observed herein, as well as the information from prior works,[3, 42-47] a possible reaction pathway (Figure. 5a) that the formation of acetate via the CO insertion mechanism (an Eley-Rideal mechanism) is proposed. The CO adsorbed on the active site generates *COH or *CHO species via proton-coupled-electron-transfer (PCET). The adsorbed *COH species are then hydrogenated to $*CH_2$ species which serve as the selectivity determining intermediate (SDI) for the acetate formation.[43] After CO insertion to $*CH_2$, the subsequent $*CH_2CO$ intermediate is believed to be highly oriented for acetate, as only one more PCET is needed for the final product.[15] To rationalize our hypothesis, we performed the CO partial pressure experiment (Figure. 5b) and measured the Tafel slope (Figure. 5c) around the onset potential. At the high CO partial pressure region (P_{CO} > 0.3), where *CO is likely to saturate the single Cu sites, the $J_{acetate}$ still shows a positive dependence

with respect to P_{CO}. This observation indicates, unlike the Langmuir-Hinshelwood mechanism, here a direct insertion from gas-phase CO is likely to contribute to such monotonically increasing of $J_{acetate}$ vs. P_{co} at the CO saturated region.[48] The reaction order, however, is not exactly 1 at CO saturated region, which could be ascribed to a mixed rate-determining step (RDS) between Eley-Rideal and Langmuir-Hinshelwood mechanisms or a slow turnover from *CO to $*CH_2$. The Tafel slope of -118 $mV \cdot dec^{-1}$ indicates that the RDS is likely the first PCET, the *CO protonation in our case.[49] The CH_4 and acetate pathway bifurcate differently on 6.9 wt % Cu-N-C and 2.3 wt% Cu-N-C, that 6.9 wt% Cu-N-C is more selective for acetate, while more CH_4 was observed in the products from 2.3 wt% Cu-N-C. To understand such difference, we need to consider the kinetic barriers for forming subsequent $*CH_3$ and $*CH_2CO$ intermediates on the two studied Cu-N-C catalysts. From EXAFS modeling, we have found subtle differences in coordination and bonding structures of $Cu\text{-}N_3$ moieties, which cannot sufficiently explain the selectivity difference over CH_4. However, some features of the substrate might vary between the two catalysts, for example, the defects, the N-C coordination, and the form of N-dopant (pyrrole-N and pyridine-N), due to the different Cu loading. These differences could in turn deviate the charge transfer capability in low and high $Cu\text{-}N_3$ loading samples,[27, 50-51] which steer the reaction pathway between CH_4 and acetate. To elucidate the bifurcation between CH_4 and acetate pathways following $*CH_2$, future work is needed to resolve the local structure of $Cu\text{-}N_3$ based catalysts and calculate the kinetic barriers for $*CH_3$ and $*CH_2CO$ intermediates.

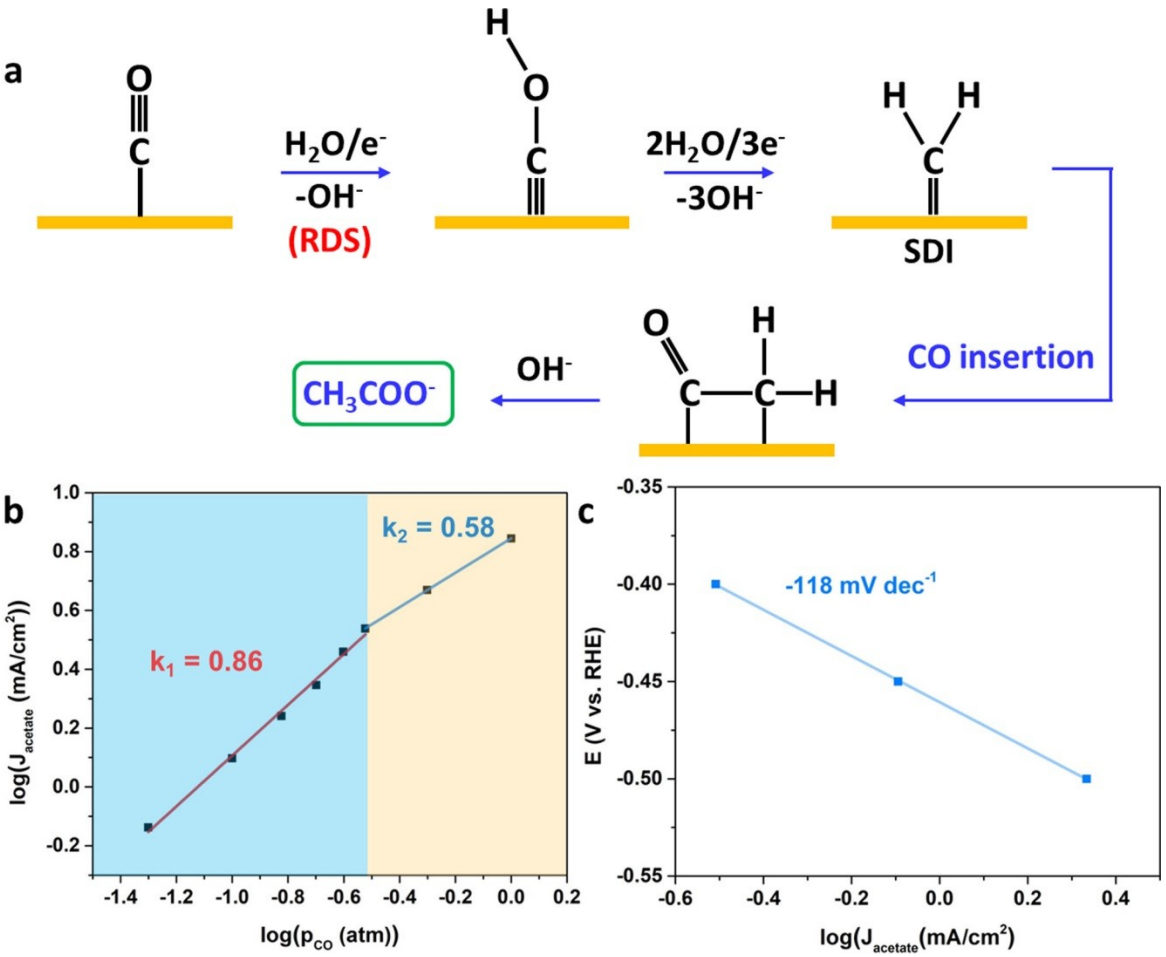

Figure 5. Mechanism study. (a) Proposed reaction pathway of the electroreduction of CO to the acetate on Cu-N-C electrocatalyst. (b) Acetate partial current densities over the partial pressure of CO (balanced with Ar). (c) Tafel analysis for acetate.

Conclusion

In summary, we developed a strategy to pyrolyze the supramolecular assembly to synthesize the atomically dispersed Cu atoms on porous nitrogen-doped carbon materials with an unsaturated coordination structure of Cu-N_2 and Cu-N_3. In electrochemical CO reduction, an overall C_{2+} selectivity (over C_1) of ~100%, a maximum FE of 30% for acetate production and an acetate partial current density of 48 mA cm^{-2} were achieved in 1 M KOH on 6.9 wt% Cu-N-C catalyst, which were the highest among the previously reported Cu-based SSCs towards acetate production. We propose that the high selectivity of acetate formation on Cu-N-C catalysts may be attributed to the CO insertion mechanism. This work offers insights into the design and development of catalysts for C_{2+} production and uncovering the C_{2+} formation mechanism which leads to the rational design of the electrocatalysts for CO_2 and CO reduction, contributing to the chemical upgrade under the hydrogen economy.

ASSOCIATED CONTENT

Supporting Information

The Supporting Information is available free of charge at https://

Experimental sessions, description of method, XRD, SEM, STEM, and XAS of Cu-N-C.

AUTHOR INFORMATION

Corresponding Author

Chao Wang - Department of Chemical and Biomolecular Engineering, Johns Hopkins University, Baltimore, Maryland 21218, United States

Email: chaowang@jhu.edu

Yijin Kang - Institute of Fundamental and Frontier Sciences, University of Electronic Science and Technology of China, Chengdu, Sichuan 610054, China

Email: kangyijin@uestc.edu.cn

Authors

Xianbiao Fu - Institute of Fundamental and Frontier Sciences, University of Electronic Science and Technology of China, Chengdu, Sichuan 610054, China; Department of Chemical and Biomolecular Engineering, Johns Hopkins University, Baltimore, Maryland 21218, United States

Yuxuan Wang - Department of Chemical and Biomolecular Engineering, Johns Hopkins University, Baltimore, Maryland 21218, United States

Hao Shen - Department of Chemical and Biomolecular Engineering, Johns Hopkins University, Baltimore, Maryland 21218, United States

Yanan Yu-

Fei Xu - Department of Chemical and Biomolecular Engineering, Johns Hopkins University, Baltimore, Maryland 21218, United States

Guangye Zhou - Department of Chemical and Biomolecular Engineering, Johns Hopkins University, Baltimore, Maryland 21218, United States

Wenjun Xie - Department of Chemistry, Nankai University, Tianjin 300071, P.R. China; Department of Chemical and Biomolecular Engineering, Johns Hopkins University, Baltimore, Maryland 21218, United States

Ruixuan Qin - College of Chemistry and Chemical Engineering, Xiamen University, Xiamen 361005, P.R. China

Chaochao Dun - The Molecular Foundry, Lawrence Berkeley National Laboratory, Berkeley, CA, 94720, US

Yisheng Liu - Advanced Light Source, Lawrence Berkeley National Laboratory, Berkeley, California 94720, United States

Jinghua Guo - Advanced Light Source, Lawrence Berkeley National Laboratory, Berkeley, California 94720, United States

Qin Yue - Institute of Fundamental and Frontier Sciences, University of Electronic Science and Technology of China, Chengdu, Sichuan 610054, China

Jeffrey J. Urban - The Molecular Foundry, Lawrence Berkeley National Laboratory, Berkeley, CA, 94720, US

Notes

The authors declare no competing financial interests.

Acknowledgment

The work is supported by the National Natural Science Foundation of China, under Award 21701153 and 21773023, and Sichuan Science and Technology Program□NO. 2020YJ0243).

References

(1) Ross, M. B.; De Luna, P.; Li, Y. F.; Dinh, C. T.; Kim, D.; Yang, P.; Sargent, E. H. Designing materials for electrochemical carbon dioxide recycling. *Nat. Catal.* **2019,** *2* (8), 648-658.

(2) Birdja, Y. Y.; Perez-Gallent, E.; Figueiredo, M. C.; Gottle, A. J.; Calle-Vallejo, F.; Koper, M. T. M. Advances and challenges in understanding the electrocatalytic conversion of carbon dioxide to fuels. *Nat. Energy.* **2019,** *4* (9), 732-745.

(3) Jiao, Y.; Zheng, Y.; Chen, P.; Jaroniec, M.; Qiao, S. Z. Molecular Scaffolding Strategy with Synergistic Active Centers To Facilitate Electrocatalytic CO_2 Reduction to Hydrocarbon/Alcohol. *J. Am. Chem. Soc.* **2017,** *139* (49), 18093-18100.

(4) Tackett, B. M.; Gomez, E.; Chen, J. G. G. Net reduction of CO_2 via its thermocatalytic and electrocatalytic transformation reactions in standard and hybrid processes. *Nat. Catal.* **2019,** *2* (5), 381-386.

(5) Larrazabal, G. O.; Martin, A. J.; Perez-Ramirez, J. Building Blocks for High Performance in Electrocatalytic CO_2 Reduction: Materials, Optimization Strategies, and Device Engineering. *J. Phys. Chem. Lett.* **2017,** *8* (16), 3933-3944.

(6) Wu, Y. S.; Jiang, Z.; Lu, X.; Liang, Y. Y.; Wang, H. L. Domino electroreduction of CO2 to methanol on a molecular catalyst. *Nature.* **2019,** *575* (7784), 639-642.

(7) Nitopi, S.; Bertheussen, E.; Scott, S. B.; Liu, X. Y.; Engstfeld, A. K.; Horch, S.; Seger, B.; Stephens, I. E. L.; Chan, K.; Hahn, C.; Norskov, J. K.; Jaramillo, T. F.; Chorkendorff, I. Progress and Perspectives of Electrochemical CO_2 Reduction on Copper in Aqueous Electrolyte. *Chem. Rev.* **2019,** *119* (12), 7610-7672.

(8) Li, F. W.; Thevenon, A.; Rosas-Hern?ndez, A.; Wang, Z. Y.; Li, Y. L.; Gabardo, C. M.; Ozden, A.; Dinh, C. T.; Li, J.; Wang, Y. H.; Edwards, J. P.; Xu, Y.; McCallum, C.; Tao, L. Z.; Liang, Z. Q.; Luo, M. C.; Wang, X.; Li, H. H.; O'Brien, C. P.; Tan, C. S.; Nam, D. H.; Quintero-Bermudez, R.; Zhuang, T. T.; Li, Y. G. C.; Han, Z. J.; Britt, R. D.; Sinton, D.; Agapie, T.; Peters, J. C.; Sargent, E. H. Molecular tuning of CO_2-to-ethylene conversion. *Nature.* **2020,** *577* (7791), 509-513.

(9) Peterson, A. A.; Norskov, J. K. Activity Descriptors for CO_2 Electroreduction to Methane on Transition-Metal Catalysts. *J. Phys. Chem. Lett.* **2012,** *3* (2), 251-258.

(10) Montoya, J. H.; Shi, C.; Chan, K.; Norskov, J. K. Theoretical Insights into a CO Dimerization Mechanism in CO_2 Electroreduction. *J. Phys. Chem. Lett.* **2015,** *6* (11), 2032-2037.

(11) Karamad, M.; Tripkovic, V.; Rossmeisl, J. Intermetallic Alloys as CO Electroreduction Catalysts-Role of Isolated Active Sites. *ACS Catal.* **2014,** *4* (7), 2268-2273.

(12) Jouny, M.; Luc, W.; Jiao, F. High-rate electroreduction of carbon monoxide to multi-carbon products. *Nat. Catal.* **2018,** *1* (10), 748-755.

(13) Cuellar, N. S. R.; Wiesner-Fleischer, K.; Fleischer, M.; Rucki, A.; Hinrichsen, O. Advantages of CO over CO_2 as reactant for electrochemical reduction to ethylene, ethanol and n-propanol on gas diffusion electrodes at high current densities. *Electrochim Acta.* **2019,** *307*, 164-175.

(14) Raciti, D.; Cao, L.; Liv, K. J. T.; Rottmann, P. F.; Tang, X.; Li, C. Y.; Hicks, Z.; Bowen, K. H.; Hemker, K. J.; Mueller, T.; Wang, C. Low-Overpotential Electroreduction of Carbon Monoxide Using Copper Nanowires. *ACS Catal.* **2017,** *7* (7), 4467-4472.

(15) Luc, W.; Fu, X. B.; Shi, J. J.; Lv, J. J.; Jouny, M.; Ko, B. H.; Xu, Y. B.; Tu, Q.; Hu, X. B.; Wu, J. S.; Yue, Q.; Liu, Y. Y.; Jiao, F.; Kang, Y. J. Two-dimensional copper nanosheets for electrochemical reduction of carbon monoxide to acetate. *Nat. Catal.* **2019,** *2* (5), 423-430.

(16) Jouny, M.; Hutchings, G. S.; Jiao, F. Carbon monoxide electroreduction as an emerging platform for carbon utilization. *Nat. Catal.* **2019,** *2* (12), 1062-1070.

(17) Wang, Y. X.; Cao, L.; Libretto, N. J.; Li, X.; Li, C. Y.; Wan, Y. D.; He, C. N.; Lee, J.; Gregg, J.; Zong, H.; Su, D.; Miller, J. T.; Mueller, T.; Wang, C. Ensemble Effect in Bimetallic Electrocatalysts for CO_2 Reduction. *J. Am. Chem. Soc.* **2019,** *141* (42), 16635-16642.

(18) Zhang, W. Y.; Qin, Q.; Dai, L.; Qin, R. X.; Zhao, X. J.; Chen, X. M.; Ou, D. H.; Chen, J.; Chuong, T. T.; Wu, B. H.; Zheng, N. F. Electrochemical Reduction of Carbon Dioxide to Methanol on Hierarchical Pd/SnO_2 Nanosheets with Abundant Pd-O-Sn Interfaces. *Angew. Chem. Int. Edit.* **2018,** *57* (30), 9475-9479.

(19) Wang, Y. X.; Shen, H.; Livi, K. J. T.; Raciti, D.; Zong, H.; Gregg, J.; Onadeko, M.; Wan, Y. D.; Watson, A.; Wang, C. Copper Nanocubes for CO_2 Reduction in Gas Diffusion Electrodes. *Nano Lett.* **2019,** *19* (12), 8461-8468.

(20) Xie, H.; Wang, T. Y.; Liang, J. S.; Li, Q.; Sun, S. H. Cu-based nanocatalysts for electrochemical reduction of CO_2. *Nano Today.* **2018,** *21*, 41-54.

(21) Reske, R.; Mistry, H.; Behafarid, F.; Roldan Cuenya, B.; Strasser, P. Particle Size Effects in the Catalytic Electroreduction of CO_2 on Cu Nanoparticles. *J. Am. Chem. Soc.* **2014,** *136* (19), 6978-6986.

(22) de Arquer, F. P. G.; Dinh, C. T.; Ozden, A.; Wicks, J.; McCallum, C.; Kirmani, A. R.; Nam, D. H.; Gabardo, C.; Seifitokaldani, A.; Wang, X.; Li, Y. G. C.; Li, F. W.; Edwards, J.; Richter, L. J.; Thorpe, S. J.; Sinton, D.; Sargent, E. H. CO_2 electrolysis to multicarbon products at activities greater than 1 A cm^{-2}. *Science.* **2020,** *367* (6478), 661-666.

(23) Li, Y. F.; Kim, D.; Louisia, S.; Xie, C. L.; Kong, Q.; Yu, S.; Lin, T.; Aloni, S.; Fakra, S. C.; Yang, P. D. Electrochemically scrambled nanocrystals are catalytically active for CO_2-to-multicarbons. *P. Natl. Acad. Sci. USA.* **2020,** *117* (17), 9194-9201.

(24) Liu, S. B.; Tao, H. B.; Zeng, L.; Liu, Q.; Xu, Z. G.; Liu, Q. X.; Luo, J. L. Shape-Dependent Electrocatalytic Reduction of CO_2 to CO on Triangular Silver Nanoplates. *J. Am. Chem. Soc.* **2017,** *139* (6), 2160-2163.

(25) Feng, X. F.; Jiang, K. L.; Fan, S. S.; Kanan, M. W. Grain-Boundary-Dependent CO_2 Electroreduction Activity. *J. Am. Chem. Soc.* **2015,** *137* (14), 4606-4609.

(26) Zhang, H. N.; Li, J.; Xi, S. B.; Du, Y. H.; Hai, X.; Wang, J. Y.; Xu, H. M.; Wu, G.; Zhang, J.; Lu, J.; Wang, J. Z. A Graphene-Supported Single-Atom FeN_5 Catalytic Site for Efficient Electrochemical CO_2 Reduction. *Angew. Chem. Int. Edit.* **2019,** *58* (42), 14871-14876.

(27) Lu, B. Z.; Liu, Q. M.; Chen, S. W. Electrocatalysis of Single-Atom Sites: Impacts of Atomic Coordination. *ACS Catal.* **2020,** *10* (14), 7584-7618.

(28) Liu, H. L.; Zhu, Y. T.; Ma, J. M.; Zhang, Z. C.; Hu, W. P. Recent Advances in Atomic-Level Engineering of Nanostructured Catalysts for Electrochemical CO_2 Reduction. *Adv. Funct. Mater.* **2020,** *30* (17).

(29) Xiong, Y.; Dong, J. C.; Huang, Z. Q.; Xin, P. Y.; Chen, W. X.; Wang, Y.; Li, Z.; Jin, Z.; Xing, W.; Zhuang, Z. B.; Ye, J. Y.; Wei, X.; Cao, R.; Gu, L.; Sun, S. G.; Zhuang, L.; Chen, X. Q.; Yang, H.; Chen, C.; Peng, Q.; Chang, C. R.; Wang, D. S.; Li, Y. D. Single-atom Rh/N-doped carbon electrocatalyst for formic acid oxidation. *Nat. Nanotechnol.* **2020,** *15* (5), 390-397.

(30) Duchesne, P. N.; Li, Z. Y.; Deming, C. P.; Fung, V.; Zhao, X. J.; Yuan, J.; Regier, T.; Aldalbahi, A.; Almarhoon, Z.; Chen, S. W.; Jiang, D. E.; Zheng, N. F.; Zhang, P. Golden single-atomic-site platinum electrocatalysts. *Nat. Mater.* **2018,** *17* (11), 1033-1039.

(31) Zhao, D.; Zhuang, Z. W.; Cao, X.; Zhang, C.; Peng, Q.; Chen, C.; Li, Y. D. Atomic site electrocatalysts for water splitting, oxygen reduction and selective oxidation. *Chem. Soc. Rev.* **2020,** *49* (7), 2215-2264.

(32) Li, J. Z.; Chen, M. J.; Cullen, D. A.; Hwang, S.; Wang, M. Y.; Li, B. Y.; Liu, K. X.; Karakalos, S.; Lucero, M.; Zhang, H. G.; Lei, C.; Xu, H.; Sterbinsky, G. E.; Feng, Z. X.; Su, D.; More, K. L.; Wang, G. F.; Wang, Z. B.; Wu, G. Atomically dispersed manganese catalysts for oxygen reduction in proton-exchange membrane fuel cells. *Nat. Catal.* **2018,** *1* (12), 935-945.

(33) Jiao, J. Q.; Lin, R.; Liu, S. J.; Cheong, W. C.; Zhang, C.; Chen, Z.; Pan, Y.; Tang, J. G.; Wu, K. L.; Hung, S. F.; Chen, H. M.; Zheng, L. R.; Lu, Q.; Yang, X.; Xu, B. J.; Xiao, H.; Li, J.; Wang, D. S.; Peng, Q.; Chen, C.; Li, Y. D. Copper atom-pair catalyst anchored on alloy nanowires for selective and efficient electrochemical reduction of CO_2. *Nat. Chem.* **2019,** *11* (3), 222-228.

(34) Zheng, W. Z.; Yang, J.; Chen, H. Q.; Hou, Y.; Wang, Q.; Gu, M.; He, F.; Xia, Y.; Xia, Z.; Li, Z. J.; Yang, B.; Lei, L. C.; Yuan, C.; He, Q. G.; Qiu, M.; Feng, X. L. Atomically Defined Undercoordinated Active Sites for Highly Efficient CO_2 Electroreduction. *Adv. Funct. Mater.* **2020,** *30* (4).

(35) Ma, L. S.; Hu, W. B.; Mei, B. B.; Liu, H.; Yuan, B.; Zang, J.; Chen, T.; Zou, L. L.; Zou, Z. Q.; Yang, B.; Yu, Y.; Ma, J. Y.; Jiang, Z.; Wen, K.; Yang, H. Covalent Triazine Framework Confined Copper Catalysts for Selective Electrochemical CO_2 Reduction: Operando Diagnosis of Active Sites. *ACS Catal.* **2020,** *10* (8), 4534-4542.

(36) Zhang, T.; Verm, S.; Kim, S.; Fister, T. T.; Kenis, P. J. A.; Gewirth, A. A. Highly dispersed, single-site copper catalysts for the electroreduction of CO_2 to methane. *Journal of Electroanalytical Chemistry.* **2020**, 113862.

(37) Wang, Y. F.; Chen, Z.; Han, P.; Du, Y. H.; Gu, Z. X.; Xu, X.; Zheng, G. F. Single-Atomic Cu with Multiple Oxygen Vacancies on Ceria for Electrocatalytic CO_2 Reduction to CH_4. *ACS. Catal.* **2018,** *8* (8), 7113-7119.

(38) Zhang, T.; Zhang, D.; Han, X. H.; Dong, T.; Guo, X. W.; Song, C. S.; Si, R.; Liu, W.; Liu, Y. F.; Zhao, Z. K. Preassembly Strategy To Fabricate Porous Hollow Carbonitride Spheres Inlaid with Single Cu-N_3 Sites for Selective Oxidation of Benzene to Phenol. *J. Am. Chem. Soc.* **2018,** *140* (49), 16936-16940.

(39) Li, F.; Han, G. F.; Noh, H. J.; Kim, S. J.; Lu, Y. L.; Jeong, H. Y.; Fu, Z. P.; Baek, J. B. Boosting oxygen reduction catalysis with abundant copper single atom active sites. *Energ. Environ. Sci.* **2018,** *11* (8), 2263-2269.

(40) Yin, P. Q.; Yao, T.; Wu, Y.; Zheng, L. R.; Lin, Y.; Liu, W.; Ju, H. X.; Zhu, J. F.; Hong, X.; Deng, Z. X.; Zhou, G.; Wei, S. Q.; Li, Y. D. Single Cobalt Atoms with Precise N-Coordination as Superior Oxygen Reduction Reaction Catalysts. *Angew. Chem. Int. Edit.* **2016,** *55* (36), 10800-10805.

(41) Qin, R. X.; Liu, P. X.; Fu, G.; Zheng, N. F. Strategies for Stabilizing Atomically Dispersed Metal Catalysts. *Small Methods.* **2018,** *2* (1), 1700286.

(42) Hori, Y.; Takahashi, R.; Yoshinami, Y.; Murata, A. Electrochemical reduction of CO at a copper electrode. *J. Phys. Chem. B.* **1997,** *101* (36), 7075-7081.

(43) Zheng, Y.; Vasileff, A.; Zhou, X. L.; Jiao, Y.; Jaroniec, M.; Qiao, S. Z. Understanding the Roadmap for Electrochemical Reduction of CO_2 to Multi-Carbon Oxygenates and Hydrocarbons on Copper-Based Catalysts. *J. Am. Chem. Soc.* **2019,** *141* (19), 7646-7659.

(44) Ma, S. C.; Sadakiyo, M.; Luo, R.; Heima, M.; Yamauchi, M.; Kenis, P. J. A. One-step electrosynthesis of ethylene and ethanol from CO_2 in an alkaline electrolyzer. *J. Power. Sources.* **2016,** *301*, 219-228.

(45) Shan, J. J.; Li, M. W.; Allard, L. F.; Lee, S. S.; Flytzani-Stephanopoulos, M. Mild oxidation of methane to methanol or acetic acid on supported isolated rhodium catalysts. *Nature.* **2017,** *551* (7682), 605-608.

(46) Ren, D.; Ang, B. S. H.; Yeo, B. S. Tuning the Selectivity of Carbon Dioxide Electroreduction toward Ethanol on Oxide-Derived CuxZn Catalysts. *ACS Catal.* **2016,** *6* (12), 8239-8247.

(47) Handoko, A. D.; Chan, K. W.; Yeo, B. S. -CH_3 Mediated Pathway for the Electroreduction of CO_2 to Ethane and Ethanol on Thick Oxide-Derived Copper Catalysts at Low Overpotentials. *ACS. Energy. Lett.* **2017,** *2* (9), 2103-2109.

(48) Li, J.; Chang, K.; Zhang, H. C.; He, M.; Goddard, W. A.; Chen, J. G. G.; Cheng, M. J.; Lu, Q. Effectively Increased Efficiency for Electroreduction of Carbon Monoxide Using Supported Polycrystalline Copper Powder Electrocatalysts. *ACS Catal.* **2019,** *9* (6), 4709-4718.

(49) Liu, X. Y.; Schlexer, P.; Xiao, J. P.; Ji, Y. F.; Wang, L.; Sandberg, R. B.; Tang, M.; Brown, K. S.; Peng, H. J.; Ringe, S.; Hahn, C.; Jaramillo, T. F.; Norskov, J. K.; Chan, K. R. pH effects on the electrochemical reduction of $CO_{(2)}$ towards C_2 products on stepped copper. *Nat. Commun.* **2019,** *10*, 32.

(50) Li, D. B.; Li, X. Y.; Chen, S. M.; Yang, H.; Wang, C. D.; Wu, C. Q.; Haleem, Y. A.; Duan, S.; Lu, J. L.; Ge, B. H.; Ajayan, P. M.; Luo, Y.; Jiang, J.; Song, L. Atomically dispersed platinum supported on curved carbon supports for efficient electrocatalytic hydrogen evolution. *Nat. Energy.* **2019,** *4* (6), 512-518.

(51) Yang, Z. K.; Chen, B. X.; Chen, W. X.; Qu, Y. T.; Zhou, F. Y.; Zhao, C. M.; Xu, Q.; Zhang, Q. H.; Duan, X. Z.; Wu, Y., Directly transforming copper (I) oxide bulk into isolated single-atom copper sites catalyst through gas-transport approach. *Nat. Commun.* **2019,** *10*, 3734.